

Meson–exchange contributions to the nuclear charge operator

Antonio M. Lallena

Departamento de Física Moderna, Universidad de Granada,
E-18071 Granada, Spain

Abstract

The role of the meson–exchange current correction to the nuclear charge operator is studied in electron scattering processes involving the excitation of medium and heavy nuclei to energies up to the quasi–elastic peak. The effect of these contributions in the quasi–free electron scattering process is a reduction of at most a 3% in the longitudinal response at the energy of the peak, a value which is below the experimental error and must not be taken into account in calculations in this energy region. On the other hand, the excitation of low–lying nuclear levels of neutronic character shows, with respect to the protonic ones, a considerable effect due to the inclusion of the two–body term in the charge operator. More realistic calculations, such as those performed in the random–phase approximation framework, give rise to a mixing of one particle–one hole configurations of both kinds which reduce these effects. However, it has been found that the excitation of some of these levels is sizeably affected by the meson–exchange contribution. More precise experimental data concerning some of these states, such as e.g. the high–spin states in ^{208}Pb , could throw some light in the problem of a more feasible determination of these effects and, as a consequence, could provide an alternative procedure to obtain the charge neutron form factor.

1 Introduction

The exchange of mesons between nucleons in a nucleus, which is the mechanism responsible for the nucleon–nucleon interaction, modifies the electromagnetic interactions of the nucleus in order to maintain the current conservation. This obvious statement was pointed out by Siegert [1] soon after the exchange model of the nuclear forces was proposed by Yukawa [2]. The realization that this exchange could produce non–negligible effects on nuclear observables, such as the nuclear magnetic moments, preceded the discovery of the pion [3].

Nevertheless, it was in the early 70’s when this topic started to be of general interest. The reason for that lied in the increasing amount of experimental data of enough accuracy which begun to be available at that time.

The first clear evidence of the importance of the so–called meson–exchange currents (MEC) was identified in connection with the radiative thermal neutron capture reaction by a proton [4]. After this, processes such as the deuteron electrodisintegration at threshold [5] and the radiative neutron capture by the deuteron [6] and observables such as the magnetic form factors of ^3H and ^3He [7] could be explained both qualitative and quantitatively only after the consideration of MEC contributions.

Most of the work done since that time has been devoted to the investigation of the contributions of MEC to electromagnetic processes. These contributions have been studied in a wide range of momentum transfers, from the ground state to excitation energies corresponding the quasi–elastic (QE) peak and beyond, for light, medium and heavy nuclei and using quite different models to describe the nuclear structure. Sizeable effects have been found in a number of situations, mainly in $A \leq 4$ nuclei. In medium and heavy nuclei, MEC produce rather small effects what has been linked to the absence of short–range correlations of tensor type in the models commonly used to describe the wave functions of these nuclei. [8, 9]

The reason of the focussing on multipole transitions involving the nuclear current only is related to the Siegert theorem [1] which establish that, at low momentum transfer, charge form factors are insensitive to meson exchange effects and that they can be reasonably well described by the single nucleon (impulse) approximation. However, Siegert theorem only applies in the long wavelength limit and it is possible to find situations in which also these form factors are modified by the presence of exchange effects.

In principle, and this can also be applied to transverse form factors, meson exchange contributions will be relatively bigger the larger the momentum transfer is. However, at high- q other effects such as relativistic effects or short–range correlations enter into play and make difficult a clear discrimination of the different contributions. Therefore the only way to study meson exchange effects is to look at some relatively small value of q where the contributions of the single–nucleon operators vanish accidentally. This is what happens in some of the processes above mentioned and this can also occur, and in fact it does, for charge form factors even at relatively low momentum transfer.

The first time that pion–exchange was recognized as responsible of a sizeable effect in nuclear charge form factors was in 1974 when Kloet and Tjon [10] calculated the charge form factors of the ^3H and ^3He . Basically it was impossible to attain the agreement with the experimental data in the second maximum using single–nucleon charge operator, even with relativistic wave functions. Additional calculations in light nuclei such as the deuteron [11] and ^4He [12] showed similar results.

In heavier nuclei the situation is more complicated because of the uncertainties due to the nuclear structure problem. The presence of many single–particle orbitals hides to some extent the signature of MEC effects and one should be careful with the conclusions drawn in this direction. In any case some calculations have been done in which those contributions are investigated. Radomski and Riska [13] have evaluated the pion–exchange effect in nuclear charge form factors and charge distributions of ^{16}O and ^{40}Ca and have found smaller contributions than for the α –particle. On the other hand, Negele and Riska [14] have shown that the inclusion of the pion–exchange term in the charge operator brings calculated charge form factors into better agreement with the experiment for closed–shell nuclei throughout the periodic table. Riska and Strüve [15] have calculated the charge form factors again for the same nuclei, paying attention to the role of MEC contributions in connection with medium polarization corrections and short–range effects. Finally, Lodhi and Hamilton [16] have investigated the charge form factor of ^6Li by considering MEC and short–range correlations, simultaneously. Despite the fact that in Refs. [13, 15, 16] a simple harmonic oscillator shell model has been used, the results can be considered as feasible because no important differences are found when these results are compared with those obtained with Hartree–Fock [14] or Brueckner–Hartree–Fock [17] wave functions.

In any case, not much work has been done in this context. In this paper, we want to investigate the MEC contributions to the nuclear charge operator in a variety of situations involving electromagnetic excitations of medium and heavy nuclei. The main purpose is to understand how such contributions affect the results one obtains by means of the impulse approximation (IA), which is the one widely admitted to calculate the different observables in this sector.

The organization of the paper is as follows. In Sec. II we discuss the details concerning the charge operator and the corrections to be considered. Sec. III is devoted to analyze the modification produced by the new operators in the nuclear response in the QE peak. In Sec. IV we study in detail the results obtained for the electroexcitation of bound levels in closed–shell nuclei both in a shell–model approach and in a more realistic calculation performed in the framework of the random–phase approximation (RPA). We finish by summarizing the results and giving our conclusions in the last section.

2 Model for the nuclear charge operator

Our purpose is to calculate different observables corresponding to the electron scattering by nuclei, such as cross–sections, form factors, response functions, etc. To do that it is necessary to fix both the model for the electromagnetic operator and the nuclear structure

approach to be considered to describe the nuclear states. In this section we focus our attention in the first one.

The larger contributions to the observables mentioned above are produced by the individual nucleons. In this approximation, the IA, the nuclear charge operator is

$$\rho^{\text{IA}}(\mathbf{q}, \omega) = \sum_{k=1}^A \left[G_{\text{E}}^{\text{P}}(\mathbf{q}, \omega) \frac{1 + \tau_3^k}{2} + G_{\text{E}}^{\text{N}}(\mathbf{q}, \omega) \frac{1 - \tau_3^k}{2} \right], \quad (1)$$

while the nuclear current

$$\mathbf{j}^{\text{IA}}(\mathbf{q}, \omega) = \mathbf{j}^{\text{C}}(\mathbf{q}, \omega) + \mathbf{j}^{\text{M}}(\mathbf{q}, \omega)$$

includes two terms, the convection current

$$\mathbf{j}^{\text{C}}(\mathbf{q}, \omega) = \sum_{k=1}^A \left(G_{\text{E}}^{\text{P}}(\mathbf{q}, \omega) \frac{1 + \tau_3^k}{2} + G_{\text{E}}^{\text{N}}(\mathbf{q}, \omega) \frac{1 - \tau_3^k}{2} \right) \left(\frac{\mathbf{p}_k + \mathbf{p}'_k}{2M_k} \right)$$

and the magnetization current

$$\mathbf{j}^{\text{M}}(\mathbf{q}, \omega) = \sum_{k=1}^A \frac{-i}{2M_k} \left(G_{\text{M}}^{\text{P}}(\mathbf{q}, \omega) \frac{1 + \tau_3^k}{2} + G_{\text{M}}^{\text{N}}(\mathbf{q}, \omega) \frac{1 - \tau_3^k}{2} \right) \mathbf{q} \times \boldsymbol{\sigma}^k.$$

In these equations, k runs over all the nucleons in the nucleus, G_{E}^{P} and G_{E}^{N} (G_{M}^{P} and G_{M}^{N}) are the electric (magnetic) form factors of the proton and the neutron, \mathbf{p}_k y \mathbf{p}'_k are the initial and final momenta of the k -th nucleon, M_k is its mass and \mathbf{q} and ω are the momentum and energy transferred to the nucleus in the process.

The necessity of including MEC in the nuclear current operator can be understood, in a very simple way, by means of the non-relativistic continuity equation (CE) which, in coordinate space, reads

$$\nabla \cdot \mathbf{j} = -i[H, \rho]$$

Taking into account that

$$\nabla \cdot \mathbf{j}^{\text{IA}} \equiv \nabla \cdot \mathbf{j}^{\text{C}} \equiv -i[T, \rho^{\text{IA}}]$$

with T the kinetic energy operator, if H includes a two-body potential, V , an additional term in the current, \mathbf{j}^{MEC} , verifying

$$\nabla \cdot \mathbf{j}^{\text{MEC}} = -i[V, \rho^{\text{IA}}]$$

must be included in order to maintain the CE. However, this equation does not provide an unique current for H and ρ given. In effect all the currents of the form $\mathbf{j} + \nabla \times \boldsymbol{\eta}$ satisfy the CE independently of the form of $\boldsymbol{\eta}$, and this happens even at the level of the IA.

Following the nomenclature of Riska [18] we call *model independent* current operators to those fixed by the CE. On the contrary, those currents not affected by this equation

are referred as *model dependent*. Out of the first type one can note the so-called seagull current,

$$\mathbf{j}^S(\mathbf{q}, \omega) = \sum_{k < j} \left\{ -i4\pi \frac{f_\pi^2}{\mu^2} F_S(\mathbf{q}, \omega) [\boldsymbol{\tau}^k \times \boldsymbol{\tau}^j]_3 \boldsymbol{\sigma}^k \frac{\boldsymbol{\sigma}^j \cdot \mathbf{q}_j}{q_j^2 + \mu^2 - \epsilon_j^2} + (k \longleftrightarrow j) \right\},$$

and pionic current,

$$\mathbf{j}^\pi(\mathbf{q}, \omega) = \sum_{k < j} i4\pi \frac{f_\pi^2}{\mu^2} F_\pi(\mathbf{q}, \omega) [\boldsymbol{\tau}^k \times \boldsymbol{\tau}^j]_3 (\mathbf{q}_k - \mathbf{q}_j) \frac{\boldsymbol{\sigma}^k \cdot \mathbf{q}_k}{q_k^2 + \mu^2 - \epsilon_k^2} \frac{\boldsymbol{\sigma}^j \cdot \mathbf{q}_j}{q_j^2 + \mu^2 - \epsilon_j^2}.$$

Between the model dependent ones the most relevant is the isobar current

$$\begin{aligned} \mathbf{j}^\Delta(\mathbf{q}, \omega) = & \sum_{k < j} \left[-i4\pi \frac{f_\pi^2}{\mu^2} F_\Delta(\mathbf{q}, \omega) \frac{\boldsymbol{\sigma}^j \cdot \mathbf{q}_j}{q_j^2 + \mu^2 - \epsilon_j^2} \left\{ [\boldsymbol{\tau}^k \times \boldsymbol{\tau}^j]_3 \mathbf{q} \times (\boldsymbol{\sigma}^k \times \mathbf{q}_j) \right. \right. \\ & \left. \left. - 4\tau_3^j \mathbf{q}_k \times \mathbf{q}_j \right\} + (k \longleftrightarrow j) \right]. \end{aligned}$$

In these equations, \mathbf{q}_k and \mathbf{q}_j are the momenta transferred to each nucleon, ϵ_k and ϵ_j the corresponding energies, μ is the pion mass and $f_\pi^2 = 0.079$ is the pion–nucleon effective coupling constant. Finally, F_S , F_π and F_Δ are the form factors of these currents.

Other MEC mechanisms, such as those corresponding to the one–rho exchange, the $\pi\rho\gamma$ and the $\pi\omega\gamma$, provide additional terms to the nuclear current operator, all of them giving, in general, small contributions to the observables of interest to us (see Ref. [19] for further details about the structure of the different operators).

A common analysis of these current terms can be carried out if an expansion in powers of v/c (or $1/M$, with M the nucleon mass) of the nuclear charge and current operators is done. Following Friar [20] it is possible to state that both the IA current as well as MEC are of order $(v/c)^1$, while the leading term in the charge operator, ρ^{IA} , is of order $(v/c)^0$. Corrections to this term are of order $(v/c)^2$ and are of relativistic type including MEC pieces. This is one of the reasons why MEC contributions have been considered extensively in the current sector and only in a few cases in the charge one. Also this indicates where to look for identifying the corresponding effects in this last case: those situations where the IA contribution vanishes or is very small.

The fact that those MEC contributions to the charge are relativistic makes that they are not fixed by the non-relativistic CE above discussed. In this sense, these charge contributions are model dependent but, fortunately, the larger effects are produced by the seagull-type term of the pion exchange current. This is given by [14, 18]

$$\begin{aligned} \rho^{\text{MEC}}(\mathbf{q}, \omega) = & \sum_{k < j} \left\{ 4\pi \frac{f_\pi^2}{\mu^2} \frac{1}{4M} \left[F_1^S(\mathbf{q}, \omega) \boldsymbol{\tau}^k \cdot \boldsymbol{\tau}^j + F_1^V(\mathbf{q}, \omega) \tau_z^j \right] \right. \\ & \left. \boldsymbol{\sigma}^k \cdot \mathbf{q} \frac{\boldsymbol{\sigma}^j \cdot \mathbf{q}_j}{q_j^2 + \mu^2 - \epsilon_j^2} + (k \longleftrightarrow j) \right\}, \end{aligned} \quad (2)$$

where F_1^S and F_1^V are the isoscalar and isovector nucleon form factors, respectively. Actual calculations have been performed by using the parametrizations of Ref. [21] for the different nucleon form factors.

Other terms involving the exchange of the ρ and ω mesons and other, such as the $\rho\pi\gamma$, produce small contributions. Calculations in the deuteron [22] and the α -particle [17] show that these additional MEC contributions are only important for very high q -transfer. The pion-exchange term dominates by more than one order of magnitude until $q \sim 5 \text{ fm}^{-1}$ where the $\rho\pi\gamma$ starts to be the leading one. In heavier nuclei the situation is similar [17] and the modifications introduced by the nuclear medium in these nuclei only change slightly the results one obtains with the bare pion exchange term alone [18].

In what follows we analyze the role of the MEC contribution to the charge operator of Eq. 2 in different electron scattering processes involving medium and heavy nuclei. Until now, the cases investigated have been the charge form factors of different nuclei such as ^{16}O and ^{40}Ca [17, 15] and ^6Li [16] and the charge densities of closed-shell nuclei throughout the periodic table [14]. The inclusion of these contributions allow, in the first case, the description of some of the diffraction minima in the charge form factor and, in the second, a better agreement with the experimental data. Nevertheless, it is worth to say that, in all the cases, the effect is rather small. We want to analyze if the same conclusion can be drawn when nuclear excitation is considered.

3 Quasi-elastic peak

The first situation we analyze concerns with the QE peak. In this energy region, the main problem deals with the longitudinal, R_L , and transverse R_T responses, which are related to the cross-section in the following way:

$$\frac{d\sigma}{d\Omega' dE'} = \sigma_M \left[\frac{q_\mu^4}{\mathbf{q}^4} R_L(q, \omega) + \left(\tan^2 \frac{\theta}{2} - \frac{q_\mu^2}{2\mathbf{q}^2} \right) R_T(q, \omega) \right].$$

Here $q^\mu = (\omega, \mathbf{q})$ is the four-momentum transferred to the nucleus, θ is the scattering angle and σ_M is the Mott cross-section,

$$\sigma_M = \left(\frac{\alpha \cos(\theta/2)}{2E \sin^2(\theta/2)} \right)^2.$$

The response functions R_L y R_T are given in terms of the transition matrix elements of the nuclear charge and current operators discussed above, between the ground state, $|0\rangle$, and final states, $|n\rangle$, of the nucleus:

$$\begin{aligned} R_L(q, \omega) &= \sum_n \delta(E_n - \omega) |\langle n | \rho(\mathbf{q}) | 0 \rangle|^2 \\ R_T(q, \omega) &= \sum_n \delta(E_n - \omega) |\langle n | \mathbf{J}_T(\mathbf{q}) | 0 \rangle|^2. \end{aligned}$$

As it is well known, these cross-sections can be described by means of a simple Fermi gas model in a very good way [23]. However, once the separation of the two responses is performed, it can be realized that neither the Fermi gas model nor more sophisticated approaches predict the experimental results: the longitudinal response is usually overestimated, while the transverse one is underestimated [24].

Different mechanisms have been considered to solve this problem (2p-2h configurations, final state interactions, relativistic effects, etc.), but though the situation of the longitudinal response is more or less understood, the same does not occur for the transverse, where the inclusion of the MEC is not sufficient to bring theory and experiment into full agreement.

What we want to investigate is the role of ρ^{MEC} in the longitudinal response. To do that we consider the Fermi gas model to describe the nucleus. In this model, the longitudinal response can be written as

$$R_L = R_L^{\text{IA}} + R_L^{\text{IA-MEC}} + R_L^{\text{MEC}},$$

where the second term (the interference one) gives the larger contribution of MEC, the last being negligible. The details of the calculation of this response for one particle-one hole (1p-1h) final states are given in Appendix A.

In our calculations we assume symmetric nuclear matter. As shown in eq. (A.1) of Appendix A, the important point is that the contribution of the interference between the IA and the MEC contributions to the charge response is negative. The effect of adding this term to the IA longitudinal response is then to reduce it, an effect which goes in the direction of reaching the experimental data.

Now we evaluate the extent of such reduction. First we calculate the responses for the Fermi momentum of nuclear matter ($k_F = 272 \text{ MeV}/c$) for different nuclei of closed-shell nuclei and for three values of the momentum transfer. To measure the effect of the MEC we analyze the relative contribution

$$r = \frac{(R_L - R_L^{\text{IA}})}{R_L^{\text{IA}}} \quad (3)$$

Table 1 shows the values obtained at the peak position in each case. It can be seen that the addition of MEC contributions only produce a small reduction of the IA response, no larger of 3%.

In any case, it is important to note (see Fig. 1) that the response $R_L^{\text{IA-MEC}}$ (long-dashed lines) presents its maxima at lower energies than R_L^{IA} (short-dashed lines) and R_L (solid lines): 40 MeV for $q = 300$ and 400 MeV/ c and 80 MeV for $q = 500$ MeV/ c . This implies a certain dependence of these MEC effects with the excitation energy.

In Fig. 2 we show (solid lines) the results obtained for the r -parameter as a function of ω . The curves correspond to the different nuclei analyzed and, at the scale of the figure, are overlapping. Thus, it is apparent that the effect does not depend on the nuclei. On

the other hand, the contribution of MEC is a small correction to the IA response and only for small energies and high momentum transfer r reach values of the order of a 10%.

The results just quoted have been obtained for $k_F = 272$ MeV/ c . A second aspect of interest is the possible dependence of the MEC effects with the values of the Fermi momentum. As it is well known, the Fermi gas model has been used to describe the QE response of finite nuclei by readjusting the value of k_F to adequate values [23]. These values can be obtained by averaging the Fermi momentum with the density [25].

In Fig. 2 we have plotted also the r -parameter calculated for ^{12}C (dashed-dotted lines) and ^{40}Ca (dashed lines), for the three momentum transfer considered and for $k_F = 215$ and 235 MeV/ c , respectively. This particular values are those provided by the procedure mentioned above. As we can see, the consideration of the new k_F values reduces the effect of the MEC and the modification of the IA longitudinal response is, at the peak energies, negligible in practice. The general trends pointed out for the nuclear matter Fermi momentum are still valid.

The main conclusion one can draw is that, though a reduction of the one-body longitudinal response in the QE peak occurs after adding the MEC contribution to the charge operator, it does not produce a sizeable effect. The smallness of these MEC contributions is due to the fact that the charge response is dominated by the proton excitations, which are by far considerably large. As noted in the Introduction, MEC effects were seen in cases where the IA term is negligible and this is not the case of the QE region. Besides, the precision of the data, clearly worst than those of the charge distributions quoted in Ref. [14], makes not necessary the consideration of these MEC effects in the calculation of such responses.

4 Electroexcitation of bound levels in closed-shell nuclei

The possibility of considering giant resonances to look for this MEC effect is not reasonable because of the difficulties inherent to this energy region in what refers to the nuclear structure. Besides, from the point of view of the dominant transitions, the mixing of different multipolarities at any energy is similar to that observed in the QE peak and one can expect the corresponding electromagnetic cross-sections to be only slightly affected by the presence of this term in the charge operator.

Low energy transitions offer, at least in principle, much more opportunities in order to investigate the modifications of the charge nuclear operator induced by MEC, because of the capacity for selecting transitions with given characteristics. In what follows we focus on these transitions. In order to minimize at most the uncertainties associated to the nuclear structure, we will consider closed-shell nuclei.

We study the process of the electroexcitation of low energy levels. The corresponding cross section is given by [26]

$$\frac{d\sigma}{d\Omega} = Z^2 \sigma_M \frac{1}{\eta} \left[\frac{q_\mu^4}{\mathbf{q}^4} |F_L(q)|^2 + \left(\tan^2 \frac{\theta}{2} - \frac{q_\mu^2}{2\mathbf{q}^2} \right) |F_T(q)|^2 \right],$$

where Z is the nuclear charge, η is the recoil factor,

$$\eta = 1 + \frac{2E}{M_T} \sin^2 \frac{\theta}{2},$$

with M_T the target nucleus mass, and $q_\mu = (\mathbf{q}, \omega)$ id the four-momentum transfers. The longitudinal, $|F_L(q)|^2$, and transverse, $|F_T(q)|^2$, form factors include the information relative to the nuclear structure. In the case of closed-shell nuclei and for a transition between the ground, $|0^+\rangle$, and the excited, $|J^\pi\rangle$, states these form factors are:

$$\begin{aligned} |F_L(q)|^2 &= \frac{4\pi}{Z^2} |\langle J^\pi \| M_J(q) \| 0^+ \rangle|^2 \\ |F_T(q)|^2 &= \frac{4\pi}{Z^2} \left\{ |\langle J^\pi \| T_J^{\text{ele}}(q) \| 0^+ \rangle|^2 + |\langle J^\pi \| T_J^{\text{mag}}(q) \| 0^+ \rangle|^2 \right\}, \end{aligned}$$

where $M_J(q)$ is the Coulomb operator and $T_J^{\text{ele}}(q)$ and $T_J^{\text{mag}}(q)$ are the electric and magnetic transverse operators. These electromagnetic multipole operators are related to the nuclear charge, $\rho(\mathbf{r})$, and current, $\mathbf{J}(\mathbf{r})$, in the following way:

$$\begin{aligned} M_{JM}(q) &= \int d\mathbf{r} j_J(qr) Y_{JM}(\hat{\mathbf{r}}) \rho(\mathbf{r}) \\ T_{JM}^{\text{ele}}(q) &= \frac{1}{q} \int d\mathbf{r} \left\{ \nabla \times [j_J(qr) \mathbf{Y}_{JJ}^M(\hat{\mathbf{r}})] \right\} \cdot \mathbf{J}(\mathbf{r}) \\ T_{JM}^{\text{mag}}(q) &= \int d\mathbf{r} j_J(qr) \mathbf{Y}_{JJ}^M(\hat{\mathbf{r}}) \cdot \mathbf{J}(\mathbf{r}). \end{aligned}$$

Here $j_J(qr)$ is a spherical Bessel function, $Y_{JM}(\hat{\mathbf{r}})$ is a spherical harmonic and $\mathbf{Y}_{JJ}^M(\hat{\mathbf{r}})$ is a vector spherical harmonic.

Taking into account the model of the nuclear charge given by eqs. (1) and (2), the longitudinal form factor, the one we are interested in, can be written as:

$$|F_L(q)|^2 = |t_{CJ}^{\text{IA}}(q) + t_{CJ}^{\text{MEC}}(q)|^2$$

with

$$t_{CJ}^a(q) = \frac{\sqrt{4\pi}}{Z} \langle J^\pi \| M_J^a(q) \| 0^+ \rangle, \quad a = \text{IA, MEC}.$$

4.1 Shell-model

First we study the closed-shell nuclei in the framework of the extreme shell-model, in which the excited levels are described as 1p-1h states. The reduced electromagnetic matrix elements t_{CJ}^a in this approximation are given by eq. (B.2) in Appendix B.

The evaluation of these reduced matrix elements requires to fix the corresponding configuration space. In this work we have used a phenomenological Woods-Saxon potential

to generate the single-particle states and energies of the nuclei considered. This potential is as follows:

$$V(r) = -\frac{V_0}{1 + e^{(r-R_0)/a_0}} - V_{\text{LS}} \frac{\hbar^2}{\mu^2 c^2} \frac{1}{r} \frac{d}{dr} \left(\frac{1}{1 + e^{(r-R_{\text{LS}})/a_{\text{LS}}}} \right) \mathbf{1} \cdot \boldsymbol{\sigma} + V_C(r),$$

where $V_C(r)$ is the Coulomb potential generated by a uniform spherical distribution with radius R_c . The parameters of this potential are adjusted in order to reproduce the single particle energies of the levels around the Fermi level and the root mean squared charge radius of the corresponding closed-shell nuclei. Table 2 shows the values used in this work.

4.1.1 ^{16}O and ^{40}Ca .

The first question we want to analyze is the behaviour of ρ^{MEC} depending on the isospin of the transition. To do that we have calculated the longitudinal form factor for the ^{16}O and ^{40}Ca nuclei and the transitions to levels with the low excitation energies (see Table 3).

The fact that in both cases $Z = N$ permits a direct comparison of the results obtained for protonic and neutronic transitions with the same quantum numbers. These are drawn in Fig. 3 and 4. Therein it is apparent that the curves including the two-body term (solid curves) are considerably modified with respect to those calculated with ρ^{IA} (dashed curves) in the case of transition of neutronic type, even at low momentum transfers. The effect of the MEC in protonic transitions are much smaller. This situation is shown in Table 4, where we give the values of the factor

$$r = \frac{|F_L|^2 - |F_L^{\text{IA}}|^2}{|F_L^{\text{IA}}|^2} \quad (4)$$

obtained, in each case, at the scattering maximum with larger strength. It can be seen that the ρ^{MEC} term dominates the longitudinal form factor in some cases of neutronic character, while the effects are practically negligible for protonic transitions.

However, these two nuclei are not expected to present purely neutronic transitions. The similitude between the energies of the 1p-1h configurations for protons and neutrons suggests actual excited states composed by a strong mixing of these configurations. As a consequence, the large difference in the strength of $|F_L|$ for both types of transitions (three orders of magnitude in ^{16}O and two in ^{40}Ca) will hide the effects of the MEC charge operator.

The idea is then to look for nuclei in which there exist excitations dominated by neutronic 1p-1h configurations. This occurs for nuclei with neutron excess. In the case of closed-shell nuclei, ^{48}Ca is the first one with this property. In what follows we analyze this nucleus and, in addition, we study the ^{208}Pb . The comparison of the results obtained for both nuclei will provide us a good information on the question we are discussing.

4.1.2 ^{48}Ca

In this nucleus, the subshell $1f_{7/2}$ is filled for neutrons and empty for protons. This situation favours the appearance of excited states predominantly neutronic at low energy and with low multipolarity. Table 5 shows the final states of 1p–1h type that can be built in the extreme shell model approach. As can be seen, the presence of the multipolarities 1^- and 3^- for both protons and neutrons with similar energies, reveals again the large mixing one can expect for these multipolarities in the actual excited states, and we have not considered them here.

On the other hand, the multipolarities with parity plus are only possible for excitations of neutronic type. This is the type of levels we are interested in. Besides we have considered the 7^- and the 5^- levels. In the first case, its high–spin character reduces the 1p–1h configurations allowed. In the second one, the expected mixing should maintain a certain degree of purity because of the energy differences (~ 2 MeV) between the corresponding 1p–1h permitted.

The results obtained for the longitudinal form factors are plotted in Fig. 5. As in the previous cases, it is evident how the effect of adding the MEC term is completely negligible in the case of protonic transitions while appreciable modifications of the one–body results are observed for transition to some neutronic final states.

In order to quantify these effects we have evaluated the r –factor, as given by eq. (4), for the scattering maxima with larger $|F_L|$ in the different transitions. The results obtained are shown in Table 6. The main aspect to be noted is that the values for r are now considerably smaller than for ^{40}Ca . However, the fact that some of the actual excitations in this nucleus are dominated by neutron 1p–1h configurations, makes it still particularly interesting. Another point to be noted is the fact that the transition to the $\pi(1f_{7/2}, 1d_{5/2}^{-1})_{5^-}$ shows a 8% effect, a value notably bigger than those obtained for ^{16}O and ^{40}Ca .

In order to elucidate if some feasible consequence can be extracted from the results obtained for this nucleus, more realistic calculations, such as, e.g., RPA, are needed. Nevertheless, we analyze the case of ^{208}Pb before going to this point.

4.1.3 ^{208}Pb

In this nucleus the levels of interest are the high–spin states. At low energy the excited states with low angular momentum show a great collectivity and then the MEC effects cannot be observed without ambiguities.

High–spin states do not present this problem because of the reduced possibilities of coupling. As a consequence, the corresponding wave functions are dominated by only a few (one or two at most in many cases) 1p–1h configurations and are ideal for the study we are carrying out.

The states of this type which have been investigated in deep are those of magnetic character. From its discovery [30] they have been considered to analyze some aspects related to the nuclear structure (partial occupation of single-particle levels [31], the role of 2p-2h configurations [32], the effective residual interaction [33], ...) or, even, to determine the MEC effects [34].

However, there exist also [35] electric states of this type, which are those we want to study here. In Table 7 the configurations giving rise to these states in the shell-model are shown. As in the case of ^{48}Ca , the possibilities of coupling of protonic configurations are strongly restricted. On the other hand, the proximity in the excitation energies predicts the mixing of 1p-1h configurations in the realistic wave functions and this will permit to study situations slightly different to those seen in the previous cases. In particular, it is interesting to point out the cases of the 10^+ states.

Fig. 6 shows the results corresponding to the transitions with $J \geq 10$. In Table 8 we have included the values of the r -factor at the maxima of F_L with larger strength. It can be seen how the inclusion of ρ^{MEC} produce notable effects in some of the neutronic transitions. Also, it is worth to point out that, again, we find a protonic transition, the one with final state $\pi(1i_{13/2}, 1h_{11/2}^{-1})_{11^-}$, with a considerably high r -value.

4.1.4 Analysis of the results

The results quoted in this section deserve some comments with respect to the regularities they show and which are of interest.

The first point, above noted, is the considerable difference between the relative effects of the MEC in the transitions of protonic and neutronic character. This is obviously due to the smallness of the one-body contribution in the neutron case. In any case, it has been observed some transitions of protonic character for which r is larger than the 3% observed in the quasi-elastic peak.

A second characteristic shown by the results is the reduction of the MEC effects as the multipolarity grows. This can be observed in those cases where various multipolarities are accesible to the same 1p-1h configuration (see the results quoted in Tables 4, 6 and 8). Then, the advantage that a priori constitutes the consideration of, e.g., the high-spin states in order both to select those of neutronic character and to minimize the number of possible 1p-1h configurations contributing to the wave functions could disappear be elliminated because of the experimental inability to detect the effects we are looking for.

Finally, a third aspect which must be pointed out is the strong variation between the MEC contributions corresponding to the two possible couplings permitted, for a given multipolarity, by the two single-particle states with same orbital angular momentum l . This situation can be observed in different cases. For example, the transitions to the levels $\nu(2p, 1f_{7/2}^{-1})_{4^+}$ in ^{48}Ca , (see Table 6 and Fig. 8) show MEC effects apreciablely bigger for the single-particle state $2p_{3/2}$ than for the $2p_{1/2}$. Same occurs in ^{208}Pb (see Table 8 and Fig. 9) with the transitions to the $\nu(2g, 1i_{13/2}^{-1})_{10^+}$ and $\nu(1j_{15/2}, 2f^{-1})_{10^+}$, where the relative variation due to the MEC is larger for the single-particle states $2g_{9/2}$ and $2f_{7/2}^{-1}$, respectively.

4.2 RPA

Once we have analyzed the basic aspects of the ρ^{MEC} operator by means of the shell-model, it is interesting to go deeper and study more realistic situations which permit the experimental identification of these effects or the determination of the conditions in which it is necessary or not to incorporate this operator to the model. To do that, and taking into account the characteristics of the nuclei we are considering, we will investigate the properties of the MEC contributions to the charge operator in the RPA framework.

This approach represents one of the procedures mostly used to describe the structure of closed-shell nuclei. In this approximation, the nuclear levels are given in terms of linear combinations of 1p-1h states which are obtained by acting with the pair p-h creation and annihilation operators on the correlated vacuum $|C\rangle$:

$$|JM\rangle = \sum_{ph} \left\{ X_J(ph) [a_p^\dagger \otimes b_h^\dagger]_M^J - (-1)^{j_p+j_h+M} Y_J(ph) [b_h \otimes a_p]_{-M}^J \right\} |C\rangle. \quad (5)$$

Here a^\dagger (a) and b^\dagger (b) are the particle and hole creation (annihilation) operators, respectively and X and Y are the RPA amplitudes. These are calculated by solving the RPA equations which involve the matrix elements of the residual interaction.

Our calculations have been performed using a residual interaction of Landau-Migdal. This is a zero-range interaction of the form

$$V_{\text{LM}}(\mathbf{r}_1, \mathbf{r}_2) = C_0 \delta(\mathbf{r}_1 - \mathbf{r}_2) \left\{ f_0^{\text{ex}} + (f_0^{\text{in}} - f_0^{\text{ex}}) \rho(\mathbf{r}_1) + f'_0 \boldsymbol{\tau}^1 \cdot \boldsymbol{\tau}^2 + g_0 \boldsymbol{\sigma}^1 \cdot \boldsymbol{\sigma}^2 + g'_0 \boldsymbol{\sigma}^1 \cdot \boldsymbol{\sigma}^2 \boldsymbol{\tau}^1 \cdot \boldsymbol{\tau}^2 \right\}$$

where $\rho(\mathbf{r})$ is the nucleon density and the parameters (see Table 9) have been taken from Ref. [29] with the change of g_0 from 0.55 to 0, a more realistic value for this type of interaction [33]. In any case it should be mentioned that the channels g_0 y g'_0 do not affect to much the calculation of electric states.

In Figs. 10 and 11 we show the spectra obtained in our calculations for ^{48}Ca and ^{208}Pb . Only the levels of interest for our study have been included for an easier analysis. As it can be seen, the calculation is reasonable for lead, despite the scarcity of data. On the other hand, the results are not satisfactory for calcium, what indicates the necessity of a more adequate interaction, in this case. This aspect is out of the purpose of this work and we will use the same interaction in both nuclei.

Once the excited states wave functions are determined, the reduced matrix elements are evaluated as given by eq. (B1). The single-particle wave functions needed for this calculation have been generated with the same Woods-Saxon potential used in the case of the shell-model.

The results obtained for the r -factor for the two nuclei we are studying are summarized in Tables 10 and 11.

In the case of ^{48}Ca (see Tables 6 and 10) it can be stated that the results are similar to those observed in the shell-model calculations, though the configuration mixing produced

by the RPA reduces considerably the MEC effects in most cases. It is worth to point out the transitions to the 7^- at 8.95 MeV and 5^- at 8.99 MeV and 11.03 MeV, which are the only in which MEC effects are above 5%. In the three cases (see Fig. 9) the corresponding transverse form factors (right panels) take values of the same order as the longitudinal ones (left panels), what could permit their separation and empirical determination. In this figure, solid (dashed) curves have been obtained with (without) the inclusion of MEC. In the transverse form factor the model for the current we have considered includes the seagull and pionic terms discussed in Sect. 2.

We can conclude that, in this case, the study of 5^- levels and the search of the 7^- could permit to go deeper in the investigation of the role of the MEC corrections to the nuclear charge in this nucleus. However, the relatively unsatisfactory results quoted above with respect to the residual interaction used, needs of a more detailed study of this aspect. Work in this direction is in progress [37].

The case of ^{208}Pb is quite different. Though the RPA calculation produce a reduction of the relative effects of MEC, as it is apparent from Figs. 9 and 13, such a reduction is not so pronounced as in ^{48}Ca . The numerical values of r shown in Table 11 favour this conclusion. In particular, the transitions to the 11^- at 6.54 MeV, 13^- at 6.55 MeV and 10^+ at 7.22 MeV states, all of them with a dominant component of neutronic character, are still showing an appreciable influence of ρ^{MEC} . Besides, the transition to the 11^- at 7.24 MeV state maintain the r -value found for its dominant configuration which is of protonic type.

On the other hand, and as it can be seen in Fig. 10, the longitudinal (left panels) and transverse (right panels) form factors for these four cases show similar order of magnitude and this makes the separation of both form factors experimentally feasible.

The importance of the configuration mixing produced by the RPA is evident in the results we have just discussed. It can be seen in Tables 10 and 11 that when the dominant configuration contributes to the wave function with an amplitude $[X_J(ph) + (-1)^J Y_J(ph)]$ far from the value 1 (that is, when the mixing is stronger), the reduction of the r -factor is considerable. This corroborates the comments made in the case of the quasi-elastic peak and indicates in a clear way that the MEC effects we are analyzing will be important only when the wave function of the excited level is sufficiently pure and, preferably, of neutronic character. These are the cases in which the ρ^{MEC} operator must be included in the calculations.

5 Summary and conclusions

In this work, the corrections introduced by the MEC in the nuclear charge operator have been analyzed in nuclear electroexcitation processes at different energy regions.

In the quasi-elastic peak, the effect of these contributions produces a diminution of the longitudinal response. Though this goes in the direction of the experimental results, the reduction is of the order of a 3% only at the peak energy, and then it is insufficient

to provide the agreement with the data. Taking into account the uncertainties introduced in the longitudinal response by the nucleon form factors and the experimental error, we can conclude that the inclusion of ρ^{MEC} in the calculations at these energies is irrelevant at present.

At low energy, MEC effects in the longitudinal form factor result to be relatively important in some cases. Calculations performed in the extreme shell-model point out the strong asymmetry of such contributions depending on the isospin of the transition: they are considerably larger in case of neutronic excitations.

On the other hand, the results obtained with calculations of RPA type reduce the MEC effects due to the configuration mixing generated. Nevertheless, it is possible to find situations in which the consideration of the ρ^{MEC} operator is mandatory.

Some of the observed aspects could be amplified if processes including polarization degrees of freedom and involving closed-shell nuclei ± 1 nucleon are used. In previous works [27, 38] it has been shown how the selection of the target polarization axis together to an adequate kinematics allow the appearance of big effects due to the MEC contributions to the current operator. In view of the fact that, as seen above, the effects in the charge (longitudinal) channel are of the same order as those in the transverse one, the mentioned processes could be specially sensible to the presence of ρ^{MEC} .

In order to finish, it is worth to note that the previous discussions have a fundamental point of uncertainty. The fact that the most relevant aspects are associated to neutronic transitions makes the electric form factor of the neutron to be one of the basic ingredients. However, the poor experimental determination of this form factor give rise to large differences between the different parametrizations available, what introduces ambiguities in the calculations of difficult evaluation. The reduction of the experimental error for the neutron electric form factor is then a basic point to bring our conclusions to a feasible practical level. In this sense, the experimental program to be developed at CEBAF is of maximum interest. On the opposite side, the careful selection of some particular transitions (such as, e.g. that to the 13^- state in ^{208}Pb) and the experimental separation of the two form factors could provide some alternative insight in the problem of the values of this form factor.

Appendix A. MEC contribution to the charge response in the Fermi gas model

In this appendix we describe the key points for the calculation of the interference response between the ρ^{MEC} operator and the IA charge one in the Fermi gas model we have considered to analyze the quasi-elastic peak region.

Assuming final states of 1p-1h type, this interference term can be written as:

$$R_L^{\text{IA-MEC}}(\mathbf{q}, \omega) = 2\text{Re} \sum_{\text{ph}} \delta(\omega + \omega_h - \omega_p) \theta(k_F - h) \theta(p - k_F) \langle \text{ph}^{-1} | \rho^{\text{IA}}(\mathbf{q}) | F \rangle \langle \text{ph}^{-1} | \rho^{\text{MEC}}(\mathbf{q}) | F \rangle^*,$$

where k_F is the Fermi momentum. Here we have used \mathbf{k} to label the single-particle state $|\mathbf{k}\omega_k s_k t_k\rangle$ which is characterized by a momentum \mathbf{k} , with $k = |\mathbf{k}|$, an energy ω_k and third spin and isospin components s_k and t_k , respectively.

Taking into account Eqs. (1) and (2), a simple calculation gives for the response of interest:

$$\begin{aligned} R_L^{\text{IA-MEC}}(\mathbf{q}, \omega) &= 4\pi \frac{f_\pi^2}{\mu^2} \sum_{t_k t_h} \frac{G_E^h(\mathbf{q}, \omega)}{M_h} B_{hkkh}^* \mathcal{R}_{t_k t_h} \\ &= -2\pi \frac{f_\pi^2}{\mu^2} \sum_{t_k t_h} \frac{G_E^h(\mathbf{q}, \omega)}{M_h} B_{hkkh}^* \mathcal{R}_{t_k t_h}^{\text{MS}}(\mathbf{q}, \omega) \end{aligned}$$

where \mathbf{k} runs over all occupied single-particle states,

$$B_{hkkh} = \left\langle \left(\frac{1}{2} t_h \right) \left(\frac{1}{2} t_k \right) \left| F_1^S(q^2) \boldsymbol{\tau}^1 \cdot \boldsymbol{\tau}^2 + F_1^V(q^2) \tau_z^1 \tau_z^2 \right| \left(\frac{1}{2} t_k \right) \left(\frac{1}{2} t_h \right) \right\rangle$$

and \mathcal{R}^{MS} represents the reduced transverse response corresponding to the interference between the magnetization and seagull currents (see Ref. [25] for details). For symmetric nuclear matter, the interference response simplifies to:

$$\begin{aligned} R_L^{\text{IA-MEC}}(\mathbf{q}, \omega) &= -2\pi \frac{f_\pi^2}{\mu^2} \frac{1}{M} \left\{ 3 \left[G_E^P(\mathbf{q}, \omega) + G_E^N(\mathbf{q}, \omega) \right] F_1^S(\mathbf{q}, \omega) \right. \\ &\quad \left. + \left[G_E^P(\mathbf{q}, \omega) - G_E^N(\mathbf{q}, \omega) \right] F_1^V(\mathbf{q}, \omega) \right\} \mathcal{R}^{\text{MS}}(\mathbf{q}, \omega). \end{aligned} \quad (\text{A.1})$$

Appendix B. MEC contribution to the charge form factor in the RPA and shell-model approach

In this appendix we give the expressions of the reduced matrix elements of the Coulomb operator which enter in the calculation of the longitudinal form factor.

In describing closed-shell nuclei in the RPA framework, the nuclear wave functions are given by Eq. (5). With this definition, and after a cumbersome calculation involving angular momentum algebra, the reduced matrix elements involved in the longitudinal form factor can be written as follows:

$$\begin{aligned} t_{C,J}^a(q) &= \frac{1}{Z} \sum [X_J^*(ph) + (-1)^J Y_J^*(ph)] (-1)^{j_p-1/2} \xi(l_p + l_h + J) \\ &\quad \hat{j}_p \hat{j}_h \hat{J} \begin{pmatrix} j_p & j_h & J \\ \frac{1}{2} & -\frac{1}{2} & 0 \end{pmatrix} \int dx x^2 j_J(qx) \mathcal{C}_{ph;J}^a(x), \end{aligned} \quad (\text{B.1})$$

where $\xi(\lambda) = 1$ or 0 according to λ be even or odd, $\hat{\lambda} = \sqrt{2\lambda + 1}$ and the functions $\mathcal{C}_{ph;J}^a(x)$ are:

$$\begin{aligned} \mathcal{C}_{ph;J}^{\text{IA}}(x) &= G_E^{ph}(q) R_p(x) R_h(x) \\ \mathcal{C}_{ph;J}^{\text{MEC}}(x) &= \frac{1}{4M_{ph}} \frac{f_\pi^2}{m_\pi^2} \sum_i \hat{j}_i^2 \mathcal{T}_{iphi} \sum_L \hat{L}^2 \left(\frac{d}{dx} + \frac{\kappa_p + \kappa_h + 2\kappa_i + 2}{x} \right) \\ &\quad \left\{ \xi(l_p + l_i + L + 1) \begin{pmatrix} j_p & j_i & L \\ \frac{1}{2} & -\frac{1}{2} & 0 \end{pmatrix}^2 I_{pi}(L, x) R_i(x) R_h(x) + (p \longleftrightarrow h) \right\}. \end{aligned}$$

Here i runs over all the single nucleon states below the Fermi level, $\kappa_\alpha = (l_\alpha - j_\alpha)(2j_\alpha + 1)$,

$$\begin{aligned} \mathcal{T}_{iphi} &= F_1^S(q)[2(\delta_{ph,\nu}\delta_{i,\pi} + \delta_{ph,\pi}\delta_{i,\nu}) + \delta_{phi,\nu} + \delta_{phi,\pi}] \\ &+ F_1^V(q)[\delta_{phi,\nu} - \delta_{phi,\pi}] \end{aligned}$$

and

$$\begin{aligned} I_{\alpha\beta}(L, x) &= \int_0^\infty dr r^2 \left\{ \left(\frac{d}{dr} + \frac{\kappa_\alpha + \kappa_\beta + 2}{r} \right) R_\alpha(r) R_\beta(r) \right\} \\ &\int_0^\infty dk k^2 \frac{2}{\pi} v_\pi(k) j_L(kr) j_L(kx). \end{aligned}$$

We are also interested in describing the nuclear states in the extreme shell-model. In this case, the excited levels a of 1p-1h character and are given as:

$$|JM\rangle = [a_p^\dagger \otimes b_h^\dagger]_M^J |0\rangle,$$

with $|0\rangle$ the Hartree-Fock vacuum. In this approach, the reduced matrix element of eq. (B.1) simplifies to

$$\begin{aligned} t_{CJ}^a(q) &= \frac{1}{Z} (-1)^{j_p-1/2} \xi(l_p + l_h + J) \hat{j}_p \hat{j}_h \hat{J} \begin{pmatrix} j_p & j_h & J \\ \frac{1}{2} & -\frac{1}{2} & 0 \end{pmatrix} \\ &\int dx x^2 j_J(qx) \mathcal{C}_{ph;J}^a(x), \end{aligned} \tag{B.2}$$

References

- [1] A.J.F. Siegert, Phys. Rev. **52** (1937) 787.
- [2] H. Yukawa, Proc. Phys. Math. Soc. Japan **17** (1935) 48.
- [3] F. Villars, Helv. Phys. Acta **20** (1947) 476.
- [4] D.O. Riska and G.E. Brown, Phys. Lett. **B38** (1972) 193.
- [5] J. Hockert, D.O. Riska, M. Gari and A. Huffman, Nucl. Phys. **A217** (1973) 14.
- [6] E. Hadjimichael, Phys. Rev. Lett. **31** (1973) 183.
- [7] A. Barroso and E. Hadjimichael, Nucl. Phys. **A238** (1975) 422.
- [8] M. Anguiano, A.M. Lallena and G. Co', Phys. Rev. **C53** (1996) 3155; M. Anguiano, Master Thesis, Universidad de Granada, 1996.
- [9] W. Leidemann and G. Orlandini, Nucl. Phys. **A506** (1990) 447; A. Fabrocini, Preprint (1996).
- [10] W.M. Kloet and J.A. Tjon, Phys. Lett. **B49** (1974) 419.
- [11] A.D. Jackson, A. Lande and D.O. Riska, Phys. Lett. **B55** (1975) 23.
- [12] J. Borysowicz and D.O. Riska, Nucl. Phys. **A254** (1975) 301.
- [13] M. Radomski and D.O. Riska, Nucl. Phys. **A274** (1976) 428.
- [14] J.W. Negele and D.O. Riska, Phys. Rev. Lett. **40** (1978) 1005.
- [15] D.O. Riska and W. Strüve, Nucl. Phys. **A399** (1983) 406.
- [16] M.A.K. Lodhi and R.B. Hamilton, Phys. Rev. Lett. **54** (1985) 646.
- [17] M. Gari, H. Hyuga and J.F. Zabolitzky, Nucl. Phys. **A271** (1976) 365.
- [18] D.O. Riska, Prog. Part. Nucl. Phys. **11** (1983) 199.
- [19] M. Chemtob and M. Rho, Nucl. Phys. **A163** (1971) 1; B. Sommer, Nucl. Phys. **A308** (1978) 263.
- [20] J.L. Friar, Phys. Rev. **C27** (1983) 2078.
- [21] G. Höhler *et al.*, Nucl. Phys. **B114** (1976) 505.
- [22] M. Gari and H. Hyuga, Nucl. Phys. **A264** (1976) 409.
- [23] E.J. Moniz, Phys. Rev. Lett. **26** (1971) 445.
- [24] B. Frois, Prog. Part. Nucl. Phys. **13** (1985) 117.

- [25] J.E. Amaro, A.M. Lallena and G. Co', Int. J. Mod. Phys. **E3** (1994) 735; J.E. Amaro, Ph. D. Thesis, Universidad de Granada, 1993 (unpublished).
- [26] T. deForest and J.D. Walecka, Adv. Phys. **15** (1966) 1.
- [27] J.E. Amaro, C. García-Recio and A.M. Lallena, Nucl. Phys. **A567** (1994) 701.
- [28] J.E. Amaro and A.M. Lallena, Nucl. Phys. **A537** (1992) 585.
- [29] G.A. Rinker and J. Speth, Nucl. Phys. **A306** (1978) 360.
- [30] J. Lichtenstadt *et al.*, Phys. Rev. Lett. **40** (1978) 1127; Phys. Rev. **C20** (1979) 497.
- [31] V.R. Pandharipande, C.N. Papanicolas and J. Wambach, Phys. Rev. Lett. **53** (1984) 1133.
- [32] S. Krewald and J. Speth, Phys. Rev. Lett. **45** (1980) 417.
- [33] A.M. Lallena, Nucl. Phys. **A489** (1988) 70; G. Co' and A.M. Lallena, Nucl. Phys. **A510** (1990) 139; N.M. Hintz, A.M. Lallena and A. Sethi, Phys. Rev. **C45** (1992) 1098.
- [34] J.S. Dehesa, S. Krewald, A.M. Lallena and T.W. Donnelly, Nucl. Phys. **A436** (1985) 573; S. Krewald, A.M. Lallena and J.S. Dehesa, Nucl. Phys. **A448** (1986) 685.
- [35] J. Lichtenstadt, Ph. D. Thesis, M.I.T., 1979.
- [36] J.E. Wise *et al.*, Phys. Rev. **C31** (1985) 1699; Y. Fujita *et al.*, Phys. Rev. **C37** (1988) 45.
- [37] M.A. Rubio, Master Thesis, Universidad de Granada, 1997 (in preparation).
- [38] S. Moraghe, J.E. Amaro, C. García-Recio and A.M. Lallena, Nucl. Phys. **A576** (1994) 553.

Tables

TABLE 1

Values of the relative effect of the MEC on the charge response (see Eq. (3)) at the peak positions, for different nuclei. The nuclear matter value for the Fermi momentum, $k_F = 272 \text{ MeV}/c$, has been used.

$q \text{ [MeV}/c]$	$\omega_{\text{max}} \text{ [MeV]}$	$r \text{ [\%]}$					
		^{12}C	^{16}O	^{40}Ca	^{48}Ca	^{90}Zr	^{208}Pb
300	50		-2.07		-2.09	-2.08	-2.09
400	90		-2.75		-2.77	-2.77	-2.78
500	150		-2.81		-2.83	-2.82	-2.84

TABLE 2

Parameters of the Woods–Saxon potential used in this work. The values for ^{12}C , ^{16}O and ^{40}Ca have been taken from Ref. [27], those of ^{48}Ca from [28] and those of ^{208}Pb from [29].

		V_0	R_0	a_0	V_{LS}	R_{LS}	a_{LS}	R_c
		[MeV]	[fm]	[fm]	[MeV]	[fm]	[fm]	[fm]
^{12}C	π	62.0	2.86	0.57	3.20	2.86	0.57	2.86
	ν	60.5	2.86	0.57	3.15	2.86	0.57	
^{16}O	π	52.5	3.20	0.53	7.00	3.20	0.53	3.20
	ν	52.5	3.20	0.53	6.54	3.20	0.53	
^{40}Ca	π	57.6	4.10	0.53	11.11	4.10	0.53	4.10
	ν	55.0	4.10	0.53	8.50	4.10	0.53	
^{48}Ca	π	59.5	4.36	0.53	8.56	4.36	0.53	4.54
	ν	50.0	4.36	0.53	7.72	4.36	0.53	
^{208}Pb	π	60.4	7.46	0.79	6.75	7.20	0.59	7.41
	ν	44.3	7.46	0.66	6.08	6.96	0.64	

TABLE 3

Final states of $1p-1h$ type considered in ^{16}O and ^{40}Ca nuclei to analyze the MEC effect in $|F_L(q)|^2$. The corresponding energies and the possible multiplicities are given.

Nucleus	Final state (1p-1h)	E_π	E_ν	J^π	
		[MeV]	[MeV]		
^{16}O	$(1d_{5/2}, 1p_{1/2}^{-1})$	11.52	11.52	3^-	
	$(2s_{1/2}, 1p_{1/2}^{-1})$	12.01	12.40	1^-	
	$(1d_{3/2}, 1p_{1/2}^{-1})$	15.11	15.36	1^-	
^{40}Ca	$(1f_{7/2}, 1d_{3/2}^{-1})$	7.24	7.27	3^-	5^-
	$(1f_{7/2}, 2s_{1/2}^{-1})$	9.77	9.74	3^-	
	$(1f_{7/2}, 1d_{5/2}^{-1})$	11.18	13.24	1^-	3^-
					5^-

TABLE 4

Values of the r -factor (see eq. (4)) for the different transitions considered in ^{16}O and ^{40}Ca , calculated at the scattering maximum with larger strength in each case.

Nucleus	Final state (1p-1h)	J^π	r [%]	
			π	ν
^{16}O	$(1d_{5/2}, 1p_{1/2}^{-1})$	3^-	1.5	11.4
	$(2s_{1/2}, 1p_{1/2}^{-1})$	1^-	0.0	-13.5
	$(1d_{3/2}, 1p_{1/2}^{-1})$	1^-	1.0	49.9
^{40}Ca	$(1f_{7/2}, 1d_{3/2}^{-1})$	3^-	1.4	17.6
		5^-	1.7	10.2
	$(1f_{7/2}, 2s_{1/2}^{-1})$	3^-	1.7	25.0
	$(1f_{7/2}, 1d_{5/2}^{-1})$	1^-	5.8	343.2
		3^-	6.2	111.1
		5^-	6.5	64.6

TABLE 5
Same as in Table 3 but for ^{48}Ca .

Final state (1p-1h)	Energy [MeV]	J^π			
$\pi(1f_{7/2}, 2s_{1/2}^{-1})$	6.18		3^-		
$\pi(1f_{7/2}, 1d_{3/2}^{-1})$	6.54		3^-	5^-	
$\pi(2p_{3/2}, 2s_{1/2}^{-1})$	9.26	1^-			
$\pi(2p_{3/2}, 1d_{3/2}^{-1})$	9.62	1^-	3^-		
$\pi(2p_{1/2}, 2s_{1/2}^{-1})$	9.69	1^-			
$\pi(1f_{5/2}, 2s_{1/2}^{-1})$	9.99		3^-		
$\pi(2p_{1/2}, 1d_{3/2}^{-1})$	10.05	1^-			
$\pi(1f_{5/2}, 1d_{3/2}^{-1})$	10.35	1^-	3^-		
$\pi(1f_{7/2}, 1d_{5/2}^{-1})$	10.78	1^-	3^-	5^-	
$\nu(2p_{3/2}, 1f_{7/2}^{-1})$	4.80		2^+	4^+	
$\nu(2p_{1/2}, 1f_{7/2}^{-1})$	6.83			4^+	
$\nu(2p_{3/2}, 1d_{3/2}^{-1})$	7.38	1^-	3^-		
$\nu(2p_{3/2}, 2s_{1/2}^{-1})$	7.40	1^-			
$\nu(1f_{5/2}, 1f_{7/2}^{-1})$	8.39		2^+	4^+	6^+
$\nu(1g_{9/2}, 1f_{7/2}^{-1})$	8.81	1^-	3^-	5^-	7^-
$\nu(2p_{1/2}, 1d_{3/2}^{-1})$	9.41	1^-			
$\nu(2p_{1/2}, 2s_{1/2}^{-1})$	9.43	1^-			
$\nu(1f_{5/2}, 1d_{3/2}^{-1})$	10.97	1^-	3^-		
$\nu(1f_{5/2}, 2s_{1/2}^{-1})$	10.99		3^-		

TABLE 6
Same as in Table 4 but for ^{48}Ca .

Final state (1p-1h)	J^π	r [%]
$\pi(1f_{7/2}, 1d_{3/2}^{-1})$	5^-	2.5
$\pi(1f_{7/2}, 1d_{5/2}^{-1})$	5^-	8.0
$\nu(2p_{3/2}, 1f_{7/2}^{-1})$	2^+	55.6
	4^+	44.1
$\nu(2p_{1/2}, 1f_{7/2}^{-1})$	4^+	-8.0
$\nu(1f_{5/2}, 1f_{7/2}^{-1})$	2^+	8.9
	4^+	3.6
	6^+	3.2
$\nu(1g_{9/2}, 1f_{7/2}^{-1})$	5^-	56.3
	7^-	37.3

TABLE 7
Same as in Table 3 but for ^{208}Pb .

Final state (1p-1h)	Energy [MeV]	J^π		
$\pi(1h_{9/2}, 1h_{11/2}^{-1})$	5.57	8^+	10^+	
$\pi(2f_{7/2}, 1h_{11/2}^{-1})$	6.47	8^+		
$\pi(1i_{13/2}, 1h_{11/2}^{-1})$	7.18	7^-	9^-	11^-
$\pi(1i_{13/2}, 2d_{5/2}^{-1})$	7.52	8^+		
$\nu(2g_{9/2}, 1i_{13/2}^{-1})$	5.07	8^+	10^+	
$\nu(1j_{15/2}, 2f_{5/2}^{-1})$	5.43	8^+	10^+	
$\nu(1j_{15/2}, 3p_{3/2}^{-1})$	5.75	8^+		
$\nu(1i_{11/2}, 1i_{13/2}^{-1})$	5.85	8^+	10^+	12^+
$\nu(1j_{15/2}, 1i_{13/2}^{-1})$	6.49	7^-	9^-	11^- 13^-
$\nu(1i_{11/2}, 2f_{7/2}^{-1})$	6.55	7^-	9^-	
$\nu(3d_{5/2}, 1i_{13/2}^{-1})$	6.63	8^+		
$\nu(2g_{9/2}, 1h_{9/2}^{-1})$	6.84	7^-	9^-	
$\nu(1j_{15/2}, 2f_{7/2}^{-1})$	7.20	8^+	10^+	
$\nu(2g_{7/2}, 1i_{13/2}^{-1})$	7.56	8^+	10^+	
$\nu(1i_{11/2}, 1h_{9/2}^{-1})$	7.62	7^-	9^-	

TABLE 8
Same as in Table 4 but for ^{208}Pb .

Transition (1p-1h)	J^π	r [%]
$\pi(1h_{9/2}, 1h_{11/2}^{-1})$	10^+	1.5
$\pi(1i_{13/2}, 1h_{11/2}^{-1})$	11^-	7.3
$\nu(2g_{9/2}, 1i_{13/2}^{-1})$	10^+	40.3
$\nu(1j_{15/2}, 2f_{5/2}^{-1})$	10^+	4.8
$\nu(1i_{11/2}, 1i_{13/2}^{-1})$	10^+	4.5
	12^+	3.8
$\nu(1j_{15/2}, 1i_{13/2}^{-1})$	11^-	49.0
	13^-	39.4
$\nu(1j_{15/2}, 2f_{7/2}^{-1})$	10^+	18.7
$\nu(2g_{7/2}, 1i_{13/2}^{-1})$	10^+	0.1

TABLE 9
Parameters of the Landau-Migdal residual interaction used in our RPA calculation.

C_0 [MeV fm ³]	f_0^{in}	f_0^{ex}	f'_0	g_0	g'_0
386.04	0.20	-2.45	1.5	0.0	0.70

TABLE 10

Same as in Table 4 but for the different RPA transitions considered in ^{48}Ca . The dominant 1p-1h configuration and the amplitude of its contribution to the form factor are also given in each case.

Energy [Mev]	J^π	r [%]	dominant (1p-1h)	$[X_J(ph) + (-1)^J Y_J(ph)]$
4.81	4^+	4.1	$\nu(2p_{3/2}, 1f_{7/2}^{-1})$	1.002
4.87	2^+	3.6	$\nu(2p_{3/2}, 1f_{7/2}^{-1})$	1.031
6.95	4^+	4.1	$\nu(2p_{1/2}, 1f_{7/2}^{-1})$	0.973
7.03	5^-	3.5	$\pi(1f_{7/2}, 1d_{3/2}^{-1})$	0.863
8.69	4^+	4.7	$\nu(1f_{5/2}, 1f_{7/2}^{-1})$	0.961
8.87	2^+	4.4	$\nu(1f_{5/2}, 1f_{7/2}^{-1})$	0.965
8.95	7^-	20.3	$\nu(1g_{9/2}, 1f_{7/2}^{-1})$	0.992
8.99	5^-	-16.1	$\nu(1g_{9/2}, 1f_{7/2}^{-1})$	0.850
9.31	6^+	4.3	$\nu(1f_{5/2}, 1f_{7/2}^{-1})$	0.976
11.03	5^-	7.0	$\pi(1f_{7/2}, 1d_{5/2}^{-1})$	0.940

TABLE 11

Same as in Table 10 but for ^{208}Pb .

Energy [Mev]	J^π	r [%]	dominant (1p-1h)	$[X_J(ph) + (-1)^J Y_J(ph)]$
5.10	10^+	2.6	$\nu(2g_{9/2}, 1i_{13/2}^{-1})$	0.996
5.51	10^+	2.2	$\nu(1j_{15/2}, 2f_{5/2}^{-1})$	0.795
5.75	10^+	1.8	$\nu(1i_{11/2}, 1i_{13/2}^{-1})$	0.592
6.49	12^+	3.5	$\nu(1i_{11/2}, 1i_{13/2}^{-1})$	1.003
6.54	11^-	14.5	$\nu(1j_{15/2}, 1i_{13/2}^{-1})$	0.984
6.55	13^-	37.5	$\nu(1j_{15/2}, 1i_{13/2}^{-1})$	0.995
6.57	10^+	1.4	$\pi(1h_{9/2}, 1h_{11/2}^{-1})$	0.723
7.22	10^+	21.4	$\nu(1j_{15/2}, 2f_{7/2}^{-1})$	0.993
7.24	11^-	7.2	$\pi(1i_{13/2}, 1h_{11/2}^{-1})$	0.983
7.77	10^+	3.9	$\nu(2g_{7/2}, 1i_{13/2}^{-1})$	0.987

Figure Captions

FIGURE 1

Longitudinal response as a function of the excitation energy ω for the ^{12}C (left) and ^{40}Ca (right) and for the three momentum transfers considered. Short-dashed curves represent the results obtained with ρ^{1A} , long-dashed curves correspond to the interference responses R_L^{int} and solid curves give the total response.

FIGURE 2

r -factor (see eq. (3)) as a function of the energy ω . With solid lines we show the values obtained for $k_F = 272$ MeV/c and for the different nuclei considered. The curves are overlapping at the scale of the figure. Dashed-dotted curves represent the results corresponding to the average values $k_F = 215$ MeV/c for ^{12}C . The same but for ^{40}Ca and $k_F = 235$ MeV/c are plotted with dashed curves.

FIGURE 3

Longitudinal form factor for the electroexcitation of the $1p-1h$ levels in ^{16}O included in Table 3. Dashed curves correspond to the calculations performed with the one-body piece of the charge density. Solid lines also include the MEC term.

FIGURE 4

Same as in Fig. 3 but for ^{40}Ca .

FIGURE 5

Same as in Fig. 3 but for the transitions in ^{48}Ca shown in Table 5.

FIGURE 6

Same as in Fig. 3 but for the transitions in ^{208}Pb shown in Table 7.

FIGURE 7

Excitation spectrum of ^{48}Ca obtained with the RPA calculation described in the text (central column). The experimental results of Ref. [36] (right column) and the levels corresponding to the shell-model (left column) are also included.

FIGURE 8

Same as in Fig. 7 but for ^{208}Pb . The experimental data are from Ref. [35].

FIGURE 9

Longitudinal (left) and transverse (right) form factor for the electroexcitation of the RPA levels of ^{48}Ca in which the r -factor is above 5%. Dashed (solid) curves correspond to the calculations performed without (with) the MEC pieces of the charge and current densities, respectively.

FIGURE 10

Same as in Fig. 9 but for ^{208}Pb .

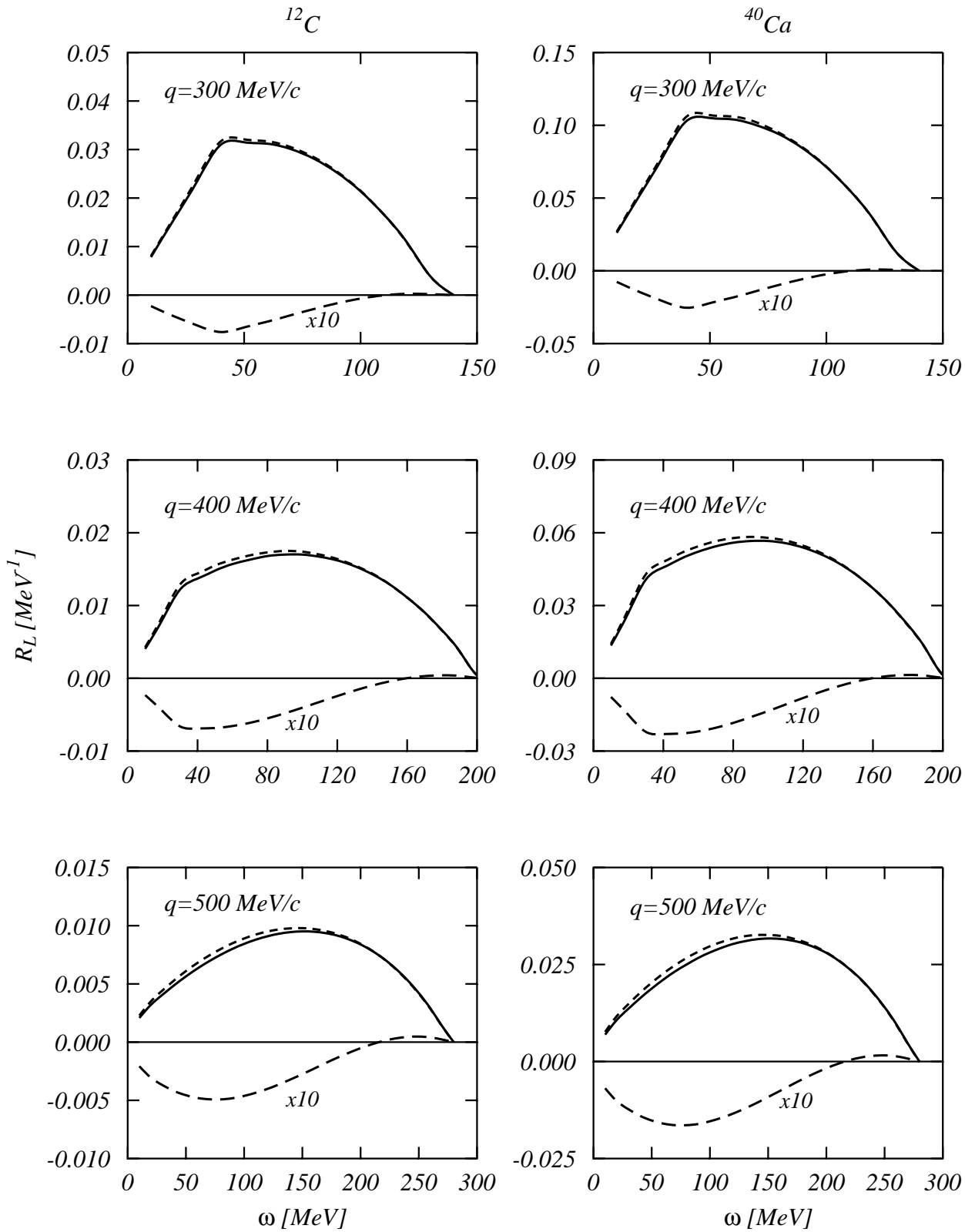


FIGURE 1

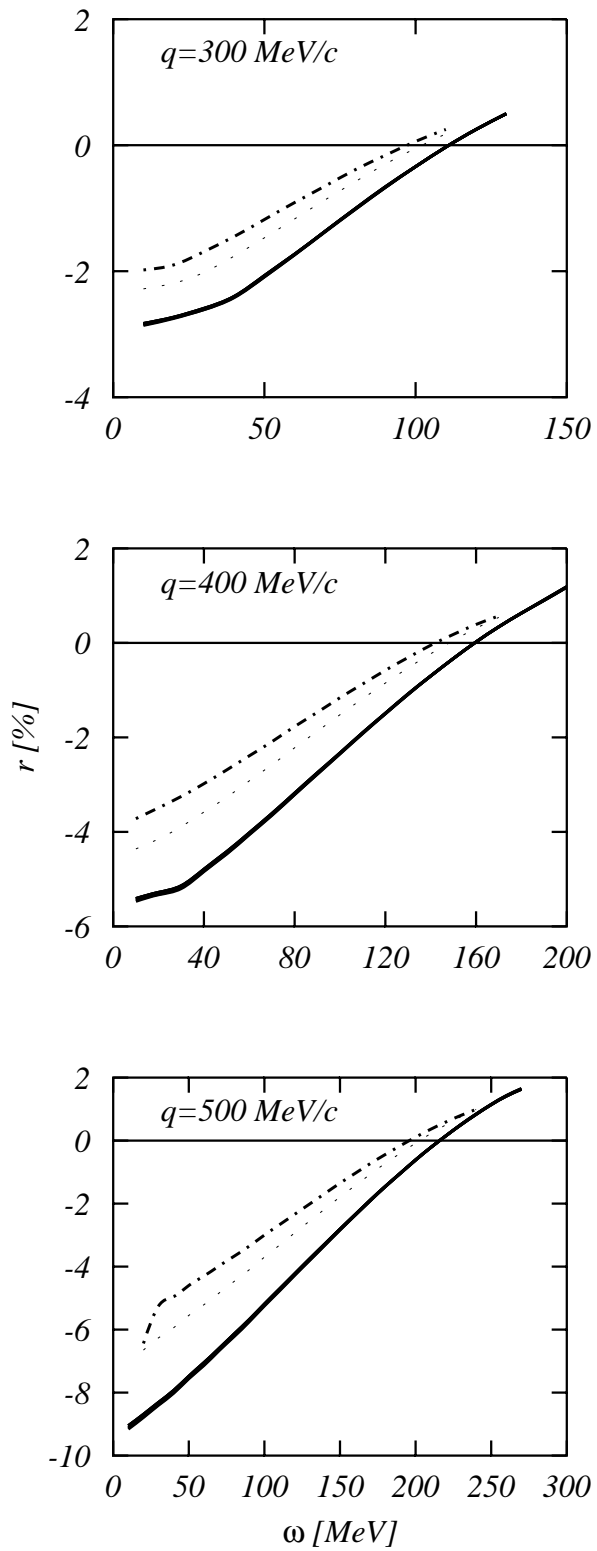


FIGURE 2

^{16}O

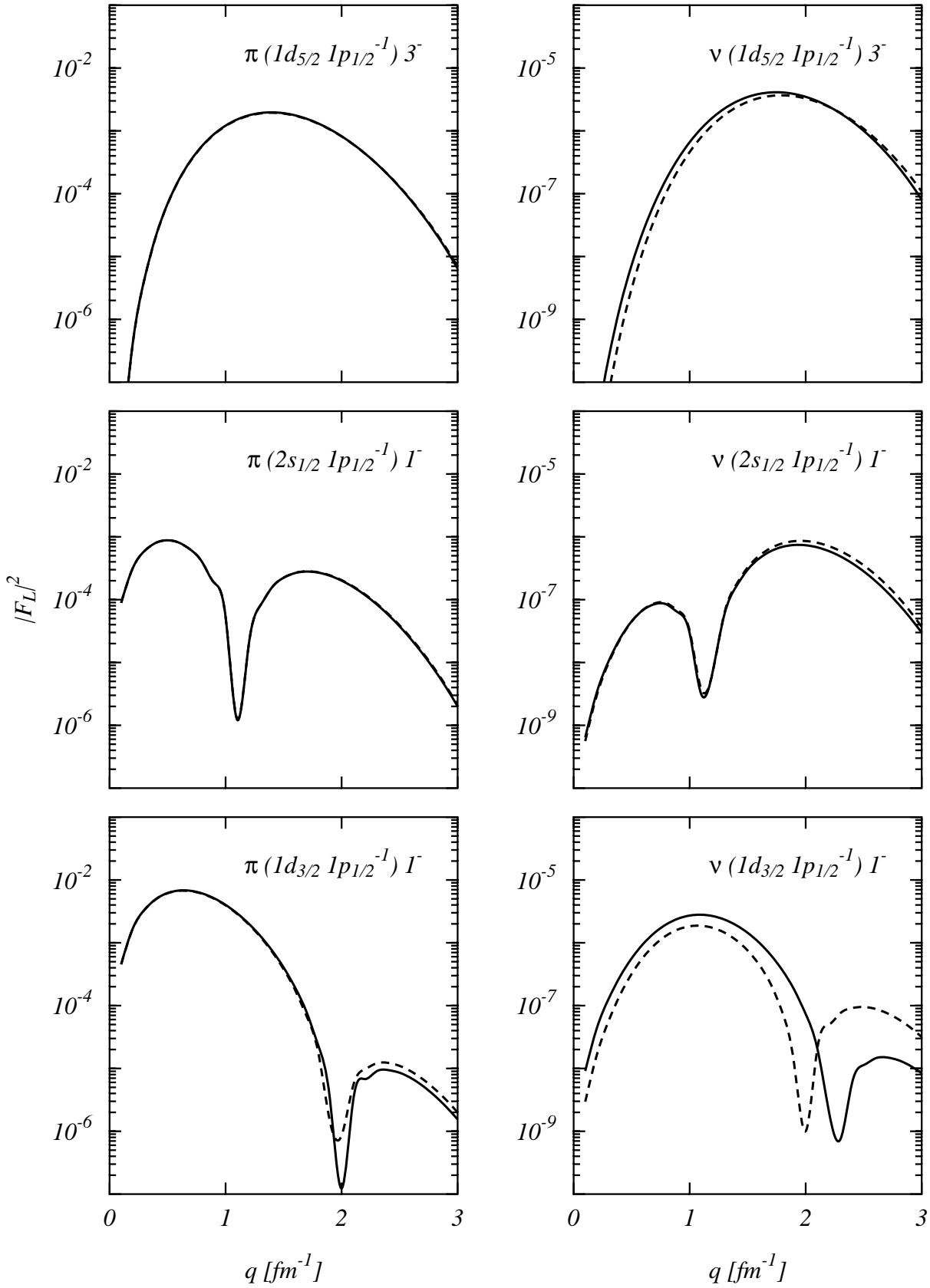


FIGURE 3

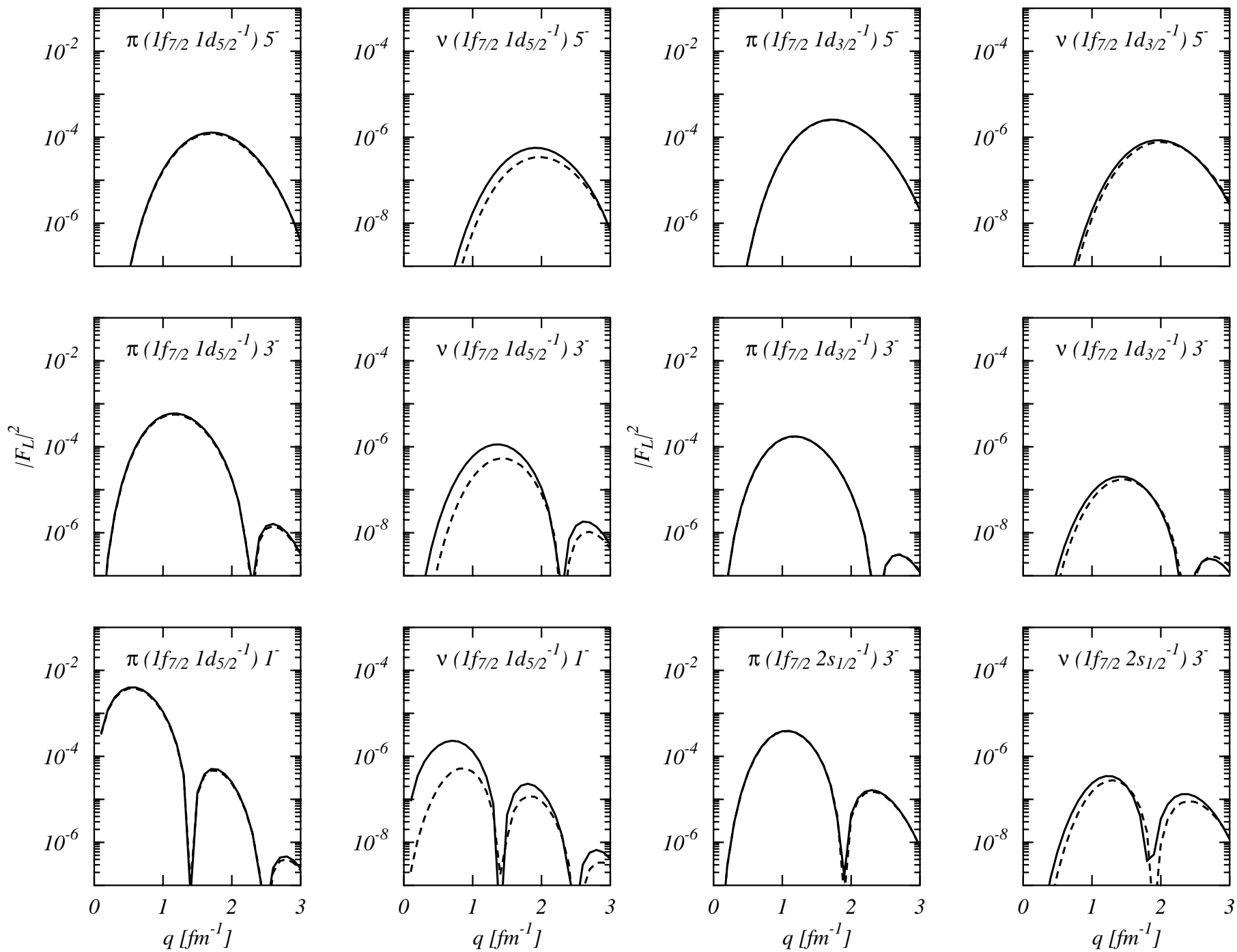
^{40}Ca 

FIGURE 4

^{48}Ca

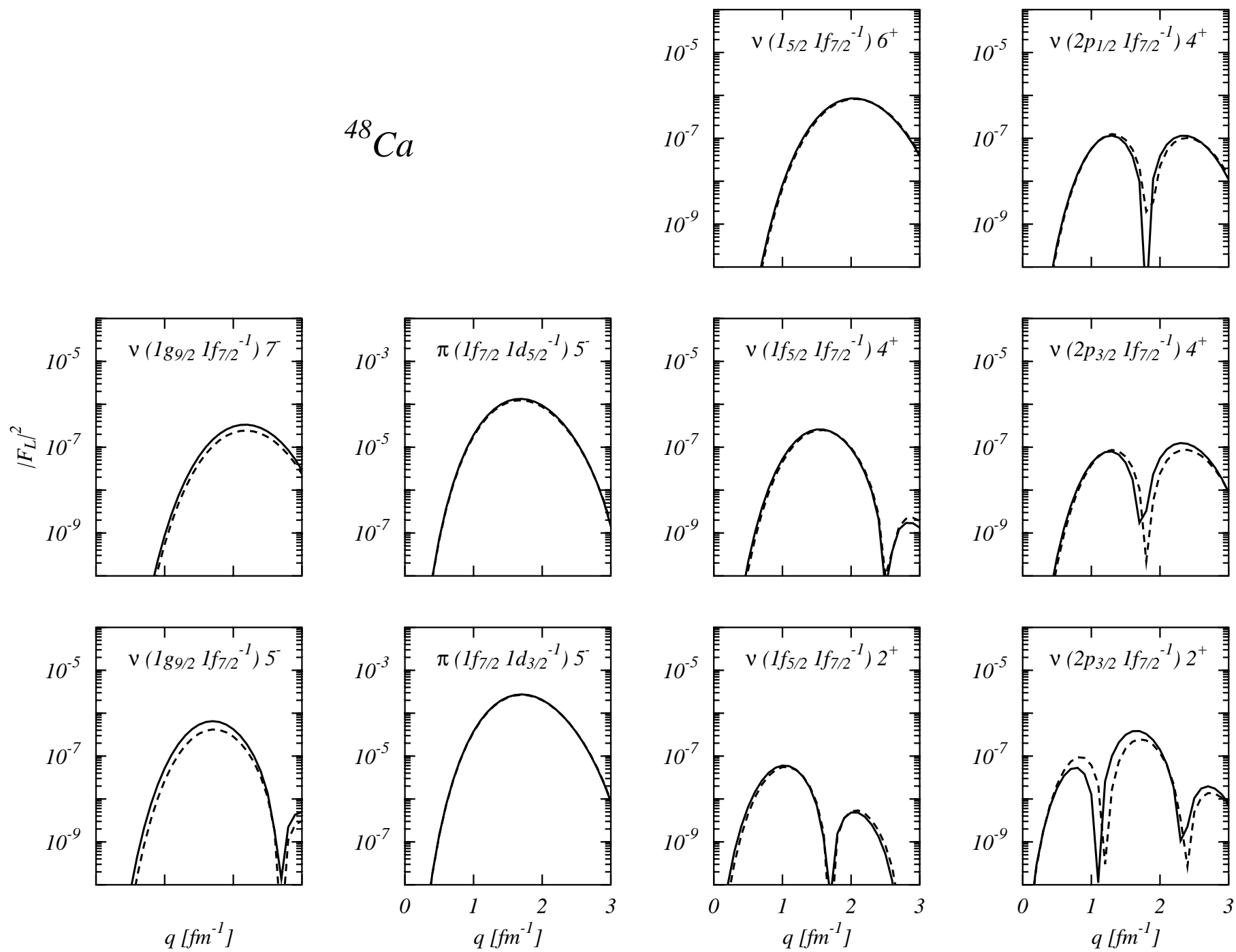


FIGURE 5

^{208}Pb

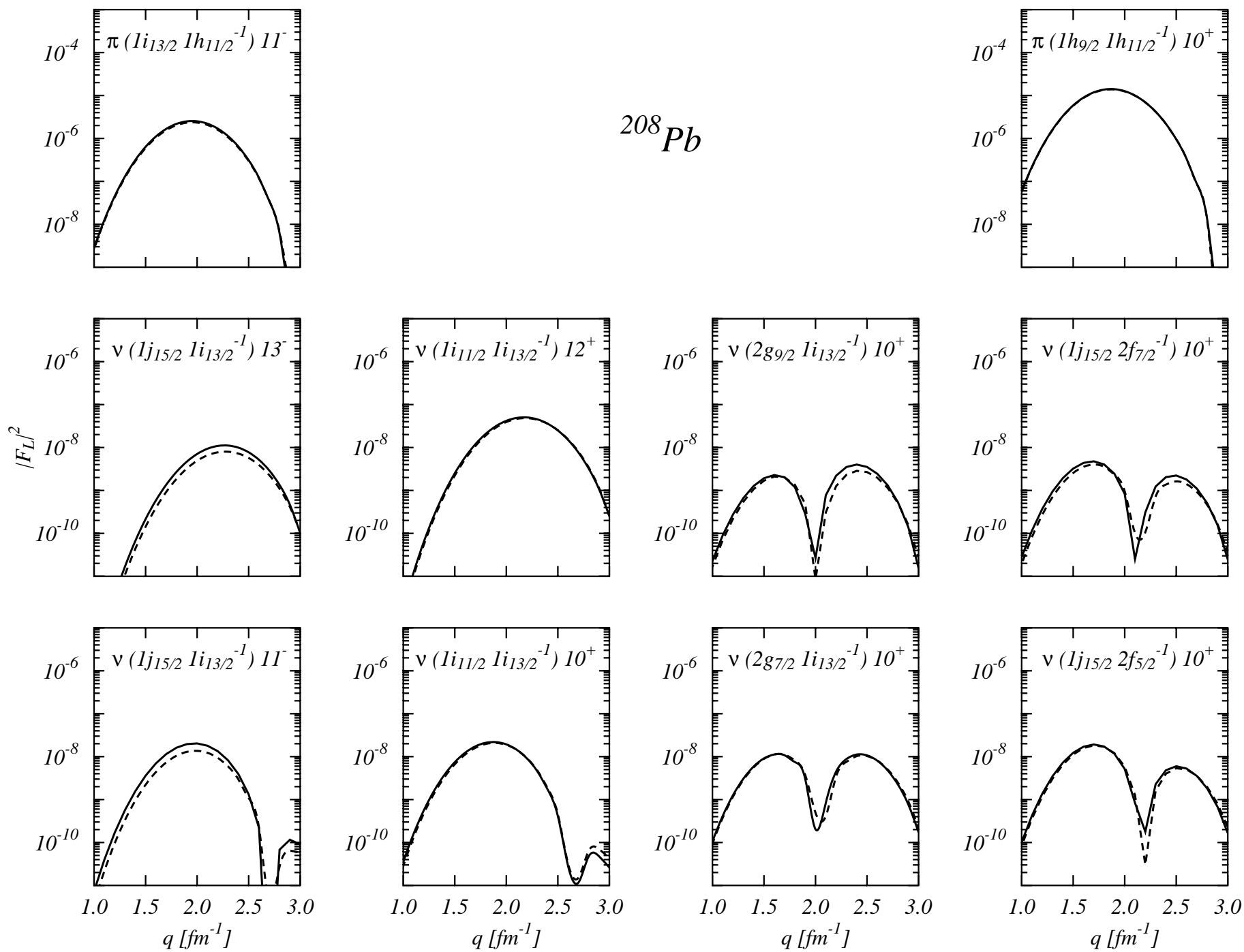


FIGURE 6

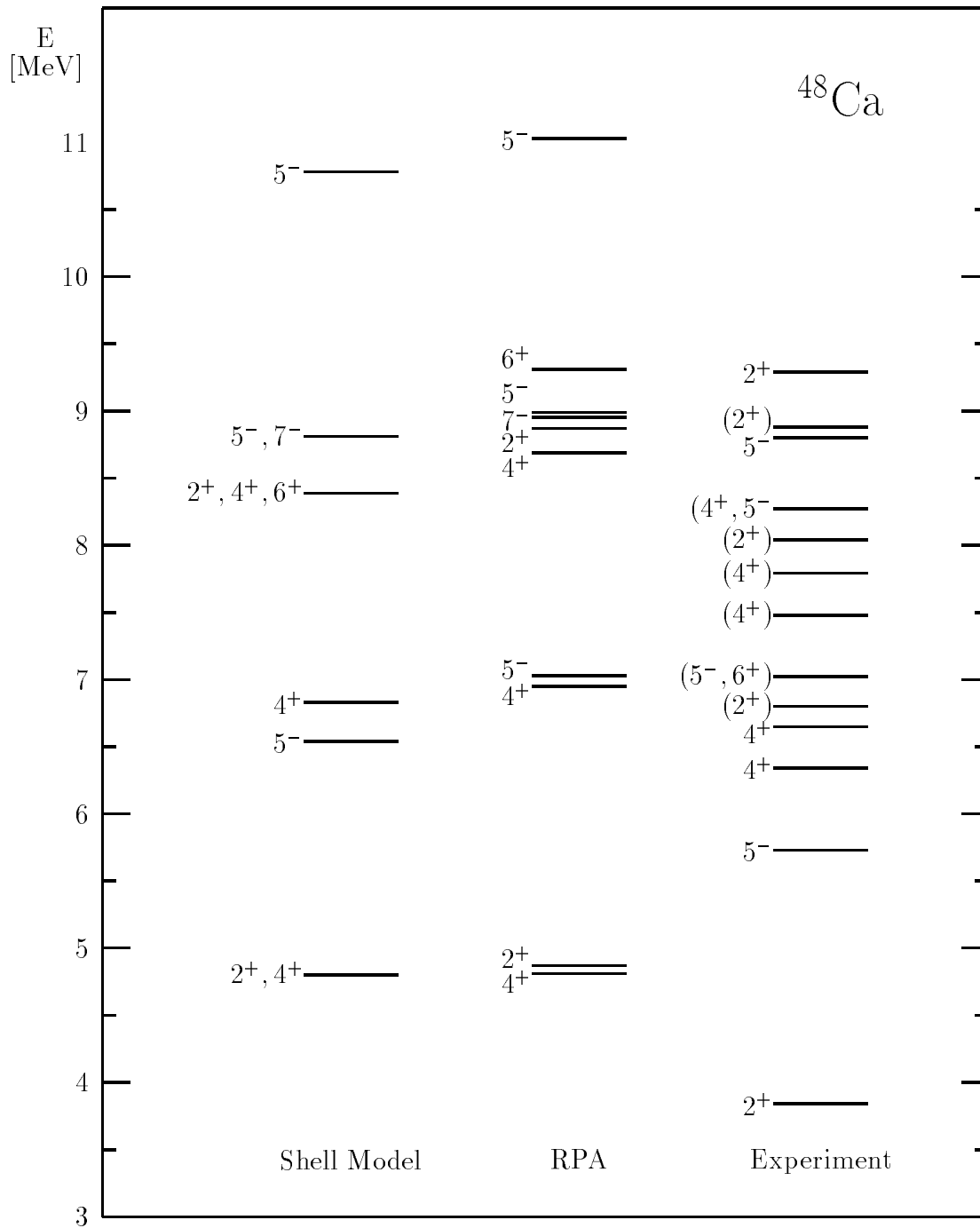


FIGURE 7

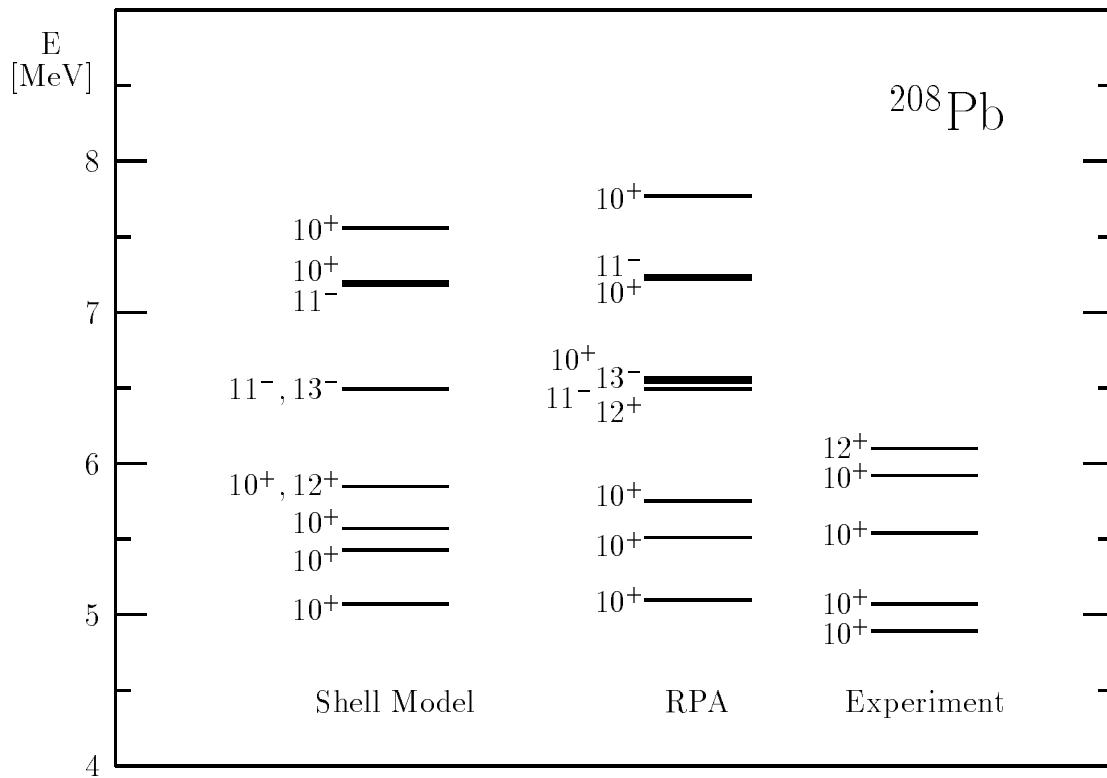


FIGURE 8

^{48}Ca

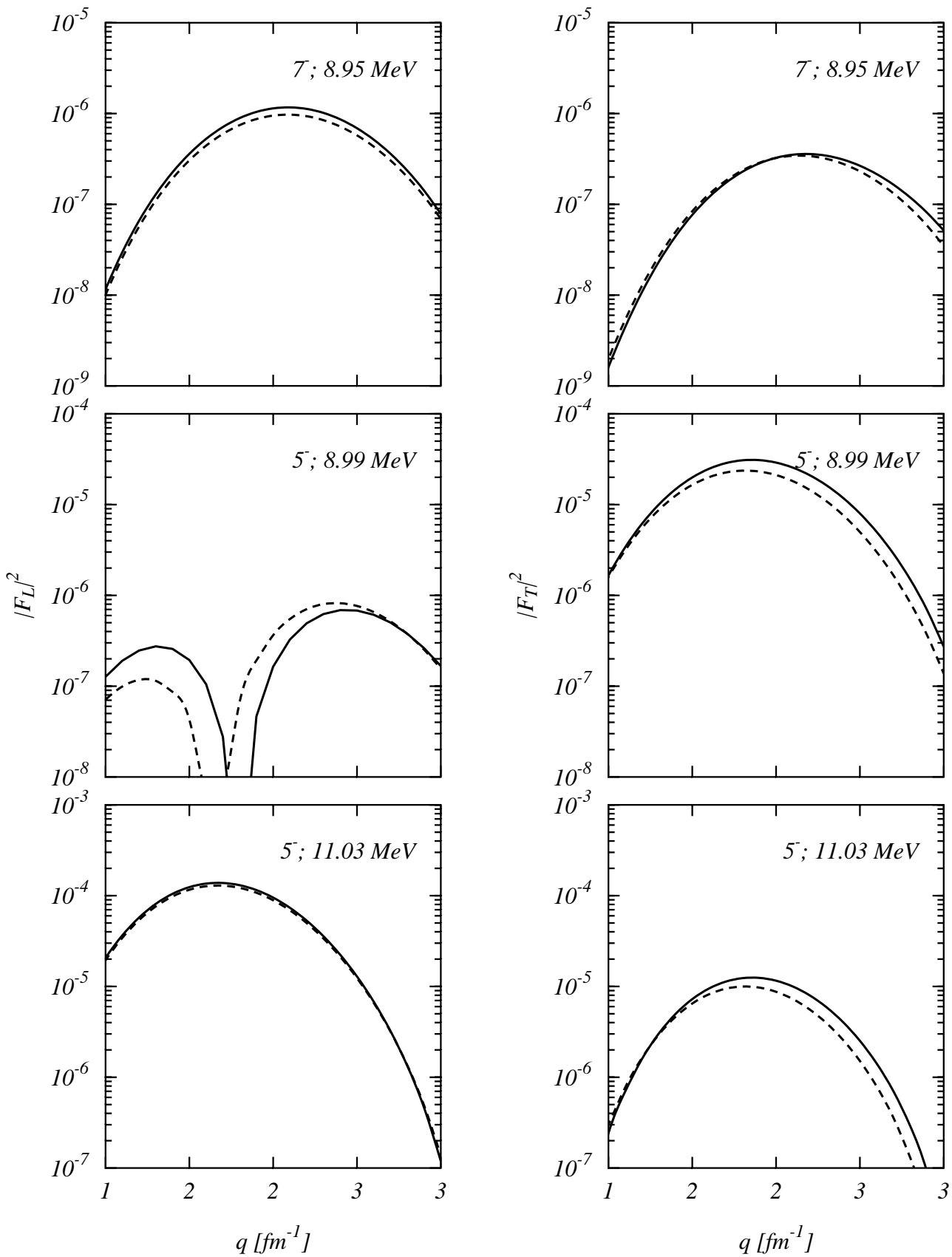


FIGURE 9

^{208}Pb

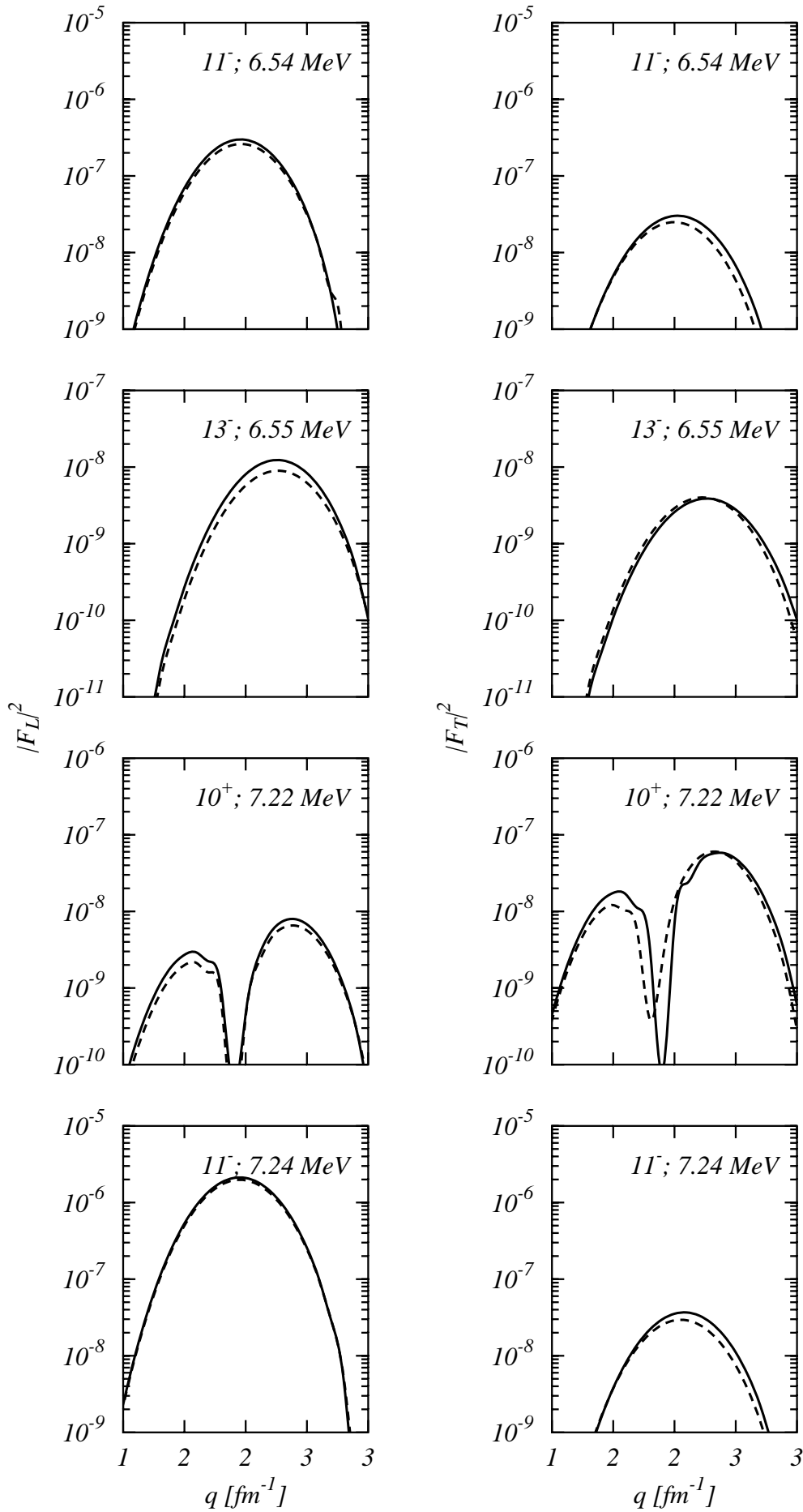


FIGURE 10